Published in final edited form as:

Exp Mol Pathol. 2016 June ; 100(3): 522–531. doi:10.1016/j.yexmp.2016.05.008.

Mitigation of nitrogen mustard mediated skin injury by a novel indomethacin bifunctional prodrug

Gabriella M. Composto[a], **Jeffrey D. Laskin**[c], **Debra L. Laskin**[a], **Donald R. Gerecke**[a], **Robert P. Casillas**[d], **Ned D. Heindel**[b], **Laurie B. Joseph**[a], and **Diane E. Heck**[e,*]

[a]Department of Pharmacology and Toxicology, Rutgers University Ernest Mario School of Pharmacy, Piscataway, NJ, United States

[b]Department of Chemistry, Lehigh University, Bethlehem, PA, United States

[c]Department of Environmental and Occupational Health, Rutgers University School of Public Health, Piscataway, NJ, United States

[d]MRIGlobal, Kansas City, MO, United States

[e]Department of Environmental Health Science, New York Medical College, Valhalla, NY, United States

Abstract

Nitrogen mustard (NM) is a bifunctional alkylating agent that is highly reactive in the skin causing extensive tissue damage and blistering. In the present studies, a modified cutaneous murine patch model was developed to characterize NM-induced injury and to evaluate the efficacy of an indomethacin pro-drug in mitigating toxicity. NM (20 μmol) or vehicle control was applied onto 6 mm glass microfiber filters affixed to the shaved dorsal skin of CD-1 mice for 6 min. This resulted in absorption of approximately 4 μmol of NM. NM caused localized skin damage within 1 d, progressing to an eschar within 2–3 d, followed by wound healing after 4–5 d. NM-induced injury was associated with increases in skin thickness, inflammatory cell infiltration, reduced numbers of sebocytes, basal keratinocyte double stranded DNA breaks, as measured by phospho-histone 2A.X expression, mast cell degranulation and increases in inducible nitric oxide synthase (iNOS) and cyclooxygenase-2 (COX-2). Wound healing was characterized by epidermal hyperplasia and marked increases in basal cells expressing proliferating cell nuclear antigen. A novel indomethacin-anticholinergic prodrug (4338) designed to target cyclooxygenases and acetylcholinesterase (AChE), was found to markedly suppress NM toxicity, decreasing wound thickness and eschar formation. The prodrug also inhibited mast cell degranulation, suppressed keratinocyte expression of iNOS and COX-2, as well as markers of epidermal proliferation. These findings indicate that a novel bifunctional pro-drug is effective in limiting NM mediated dermal injury. Moreover, our newly developed cutaneous patch model is a sensitive and reproducible method to assess the mechanism of action of countermeasures.

Graphical Abstract

*Corresponding author at: Department of Environmental Health Science SHSP, NYMC, Hospital Oval, Valhalla, NY 10595. Diane_Heck@nymc.edu (D.E. Heck PhD).

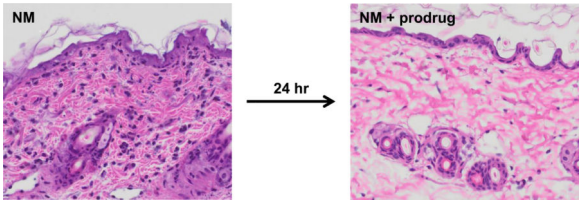

Keywords

Vesicants; Sulfur mustard; Anti-cholinergic; Epidermis; Countermeasures

Introduction

Sulfur mustard (bis(2-chloroethyl) sulfide) and nitrogen mustard (NM, bis(2-chloroethyl) methylamine, mechlorethamine) are highly toxic bifunctional alkylating agents causing epidermal and dermal damage (Shakarjian et al., 2010). In humans, depending on the dose and duration of exposure, mustards can cause acute injury, inflammation, the formation of ulcerative wounds, and blistering (Arck and Paus, 2006; Ghabili et al., 2010; Vogt et al., 1984). Generally similar responses are observed in rodent models of cutaneous exposure to sulfur mustard or NM (Tewari-Singh et al., 2013).

Key to elucidating the mechanism of action of mustards and testing potential countermeasures is the ability to generate reproducible injury in localized areas of the skin in experimental animal models. Since sulfur mustard is both lipophilic and volatile, dermal exposure can be localized using vapor cup models (Anderson et al., 2002; Joseph et al., 2011; Mershon et al., 1990). In contrast, NM is hydrophilic; thus, direct application in solvents results in spreading over a relatively large area of skin. This makes quantification of tissue damage difficult to assess (Tewari-Singh et al., 2013; Tewari-Singh et al., 2014; Vieille-Petit et al., 2015). To address this problem, cutaneous patch models have been developed. In these models, which have been used in both humans and animals, test chemicals are suspended in a matrix, which is attached to a designated area of the skin with occlusive or semi-occlusive tape (Buehler, 1994; Farage et al., 2011; Fischer and Kihlman, 1989; Nicholson and Willis, 1999). A similar model has been developed in guinea pigs to analyze hypersensitivity reactions (Buehler, 1994). Patch models have also been used to evaluate treatments for chemical burns, and as a method for delivering hydrophilic substances to the skin (Hojer et al., 2002; Hulten et al., 2004). Although many patch models can be extrapolated to human skin, there are limitations including differences between humans and animals in skin permeability of test agents, as well as their ability to induce irritation reactions (Chew and Maibach, 2003; Simon and Maibach, 1998).

In the present studies, a modified semi-occlusive patch test model employing a glass microfiber filter delivery system was developed for cutaneous NM delivery in mice; our goal was to characterize skin injury and wound healing, and to assess the efficacy of a novel bifunctional anti-inflammatory prodrug, 4338, as a potential countermeasure. The advantage of microfiber dosing is that it provides an effective method of applying NM over defined areas of the skin, making it easier to quantify tissue damage. The prodrug (4338) was

designed to target cyclooxygenases (COX), enzymes that generate proinflammatory eicosanoids, and also to target acetylcholinesterase, an enzyme mediating hydrolysis of acetylcholine (see Fig. 1 for structure). The advantage of the prodrug is that it provides a simple dosage form for two drug targets in the skin and a facilitated mechanism for onsite controlled release of the individual therapeutic components. This provides an opportunity for therapeutic properties on the skin that exceed those of the component parts. In earlier studies we showed that 4338 was effective in reducing sulfur mustard-induced edema, as well as degradation of the dermal-epidermal basement membrane; it also reduced expression of COX-2 and promoted wound re-epithelialization (Chang et al., 2014). The present studies demonstrate that our modified cutaneous patch test model is highly reproducible and can be used to effectively evaluate candidate therapeutics with the potential to mitigate vesicant-induced skin injury.

Materials and methods

Chemicals and reagents

Polyethylene glycol 400 and lanolin (C10–30 cholesterol/lano-sterol esters) were from Croda Inc., Edison, NJ. Unless otherwise indicated NM (mechlorethamine HCl) and all other chemicals were purchased from Sigma-Aldrich (St. Louis, MO). 4338 was synthesized as previously described (Young et al., 2010).

Animals and treatments

Female CD-1 mice (8 weeks; Charles River Laboratories, Wilmington, MA) were housed in filter-top microisolation cages and maintained on food and water ad libitum. Mice received humane care in compliance with the Rutgers University guidelines, as outlined in the *Guide for the Care and Use of Laboratory Animals* published by the National Institutes of Health. Mice were anesthetized by intraperitoneal injection of ketamine (80 mg/kg) and xylazine (12 mg/kg), and randomly assigned to treatment groups. The dorsal skin of the mice was shaved and then cleaned with deionized water. Six mm glass microfiber filter discs (GE Healthcare, Buckinghampshire, UK) were placed on the lumbar region of the shaved skin equal distant from the spine, and adhered with 10 μl of acetone (Fig. 2). Twenty μl of freshly prepared 1 M NM (20 μmol) in 20% deionized water/80% acetone, v/v, was then applied to the filters and immediately covered with PARAFILM® (Pechiney, Menasha, WI). Control mice received the solvent without NM. After 6 min, the filter discs were removed. In some experiments, mice were treated topically with 4338 four times per day beginning 1 h after NM. For these experiments, 20 μl of 4338 (1% in a mixture of 49.5% lanolin and 49.5% PEG400) or vehicle control was applied directly to the skin. Mice were euthanized 1–5 days post NM and 12 mm full thickness biopies of the exposure site and surrounding tissue immediately collected using a skin punch (Acuderm Inc., Ft. Lauderdale, FL). Punch biopsies were trimmed and stored in ice cold phosphate buffered saline (PBS) containing 3% paraformaldehyde/2% sucrose. The tissue was embedded in paraffin and 6 μm sections prepared and stained with hematoxylin and eosin (HE) or Gomori's trichrome containing methyl (aniline) blue, for analysis of collagen I/III (Goode Histolabs, New Brunswick, NJ). Hematoxylin and eosin stained tissue was scanned using a VS120-L100 Olympus virtual slide microscope (Waltham, MA). In some experiments, histological sections were stained

with toluidine blue O (Sigma Chemical, St. Louis MO) to visualize metachromatic/basophilic granules in mast cells. Extrusion of basophilic toluidine blue stained granules was evidence of mast cell degranulation (Joseph et al., 2011). To quantify wound thickness, measurements were performed on tissue sections using the OlyVIA 2.7 viewer software (Olympus). Skin sections were divided into 4 equal parts and measurements taken perpendicular from wound edge through the dermis, to the top surface of the hypodermis. Data were analyzed using a two way ANOVA and were expressed as mean ± S.E. ($n = 6$). A p value ≤ 0.05 was considered significant.

To estimate absorption of NM from the filter discs, NM was applied to 6 weighed control discs and allowed to dry. The filters were then weighed again to determine filter bound NM. Twelve weighed discs treated with NM that had been applied to mice (treatment discs) were removed and dried. These filters were also weighed again to determine filter bound NM post-exposures. NM absorbed was based on the difference in the weight of NM on control discs and treatment discs. In these experiments, control discs were found to contain 3.93 ± 0.35 mg NM (mean ± SD, $n = 6$) while treatment discs contained 3.18 ± 0.37 mg NM (mean ± SD, $n = 12$). Differences in NM weight between control and treatment discs was 0.75 mg. Thus, approximately 20% of the NM applied to the skin was absorbed (~4 μmoles or ~0.14 μmoles NM/mm^2 of the filters discs).

Immunostaining

For immunohistochemistry, tissue sections (6 μm) were deparaffinized, and blocked with 25%–100% normal goat serum (Invitrogen, Grand Island, NY) at room temperature for 2 h. Sections were then incubated overnight at 4 °C with rabbit affinity purified polyclonal antibodies against phospho-H2A.X (Ser139, Cell Signaling, 1:50, Boston, MA), cyclooxygenase-2 (COX-2, Abcam, 1:200, Cambridge, MA), inducible nitric oxide synthase (iNOS, Abcam, 1:150), proliferating cell nuclear antigen (PCNA, Abcam, 1:500), or control rabbit IgG (Prosci, Atlanta, GA). After washing, the sections were incubated at room temperature for 30 min with biotinylated goat anti-rabbit secondary antibody (Vector Labs, Burlingame, CA). Antibody binding was visualized using a DAB Peroxidase Substrate Kit (Vector Labs).

Results

Effects of NM on mouse skin

In initial studies we characterized histopathological changes in the skin following NM exposure. Whereas damage was primarily limited to the area beneath the 6 mm filters, areas of inflammation typically extended 1–2 mm beyond the exposure site (Fig. 2, upper panel). Gross examination of the tissue revealed redness and swelling of the skin within 1–2 days, followed by the development of an indurated crusty wound after 2–3 days, and wound healing by 4–5 days (Fig. 2, lower panels). Histologically, control skin consisted of a relatively thin epidermis 2–3 cell layers thick, with a contiguous stratum corneum (Fig. 3 and Fig. 4, CTL). Loss of the stratum corneum was evident 1–2 days post-NM, along with an inflammatory cell infiltrate (Fig. 3, left panel). Two-three days post-NM, an eschar developed over the wound site, accompanied by a general loss of dermal appendages

including sebaceous glands and hair follicles. This was associated with an increase in wound and epidermal thickness (Fig. 3, left panels and Fig. 4). A thickened hyperplastic wound persisted in the skin 3–5 days post-NM. At this time, the eschar sloughed off leaving an acanthotic epidermis (Fig. 3, left panels). Trichrome staining showed that NM treatment resulted in collagen deposition in the papillary dermis within 2 days (Fig. 5, left panels). Three to four days post NM, hemorrhage was evident within the thickened reticular dermis with hyperkeratosis superior to the hyperplastic epidermis. Three-five days post NM, epidermal hyperplasia was also observed (Fig. 5, left panels). After 5 days, hyperkeratosis was still evident, along with increased collagen deposition in both the reticular and papillary dermis (Fig. 5, left panels).

As a bifunctional alkylating agent, NM is known to induce double stranded DNA breaks (Clingen et al., 2008). Phosphorylation of histone H2A.X, a variant of histone H2A, creates a recognition domain critical for DNA repair and is a marker of DNA damage (Jowsey et al., 2009; Mah et al., 2010). Little or no phospho-H2A.X was evident in control skin (Fig. 6, CTL). NM caused a marked increase in phospho-H2A.X expression in the nuclei of basal and suprabasal cells of the interfollicular epidermis and the outer root sheath of hair follicles within 1–3 days (Fig. 6, left panel). Two-three days post-NM, phospho-H2A.X was also evident in infiltrating inflammatory cells beneath the eschar extending into the underlying dermis (Fig. 6, left panel). Interestingly, phospho-H2A.X persisted in the skin, primarily in the basal and suprabasal cells of the neoepidermis, for at least 5 days post NM (Fig. 6, left panels).

Nitric oxide is a reactive proinflammatory mediator generated in skin cells via an inducible isoform of nitric oxide synthase (iNOS) (Cals-Grierson and Ormerod, 2004; Heck et al., 1992). In control skin, iNOS expression was only noted in sebaceous glands (Fig. 7); 1–2 days following NM, iNOS was evident in interfollicular epidermis and outer root sheath cells (Fig. 7, left panel). After 3–5 days, iNOS appeared in both the hyperplastic neoepidermis and outer root sheath cells (Fig. 7, left panel). COX-2 is an enzyme that generates pro-inflammatory prostaglandins (Lee et al., 2003). Low level COX-2 expression was detected in basal cells of the epidermis, outer root sheath cells and sebaceous glands in control tissue (Fig. 8 and not shown). COX-2 increased in basal cells and dermal inflammatory cells 1–2 days post NM (Fig. 8, left panels). After 2 days, COX-2 expression was also increased in the epidermis and inflammatory cell infiltrate at the wound edge (Fig. 8, left panel). Three-five days post NM, COX-2 was also evident in the hyperplastic neoepidermis (Fig. 8, left panels).

Evidence suggests that mast cells in the skin play a role in the release of mediators important in inflammation and wound repair (Joseph et al., 2011; Tewari-Singh et al., 2009). In control skin mast cells were identified in the dermis, adjacent to dermal appendages and at the dermal/epidermal junction (Fig. 9, upper panels and not shown). Approximately 23–36% of the mast cells were found to be degranulated. NM treatment had no effect on the number of mast cells in the skin at the dermal/epidermal junction (Fig. 9, lower panel). However, a marked increase in degranulated mast cells (50–75%) was noted after NM treatment.

PCNA, a marker of cellular proliferation and wound repair (Moldovan et al., 2007; Park et al., 2015) was expressed in basal cells in control mouse skin (Fig. 10). NM treatment resulted in increased expression of PCNA in basal keratinocytes, as well as in inflammatory cells in the dermis within 1 day (Fig. 10, left panels). Two-three days post-NM, PCNA was detected in infiltrating inflammatory cells beneath the eschar at the dermal/epidermal junction; after 4–5 days, PCNA expression was evident within basal keratinocyte nuclei of the neoepidermis (Fig. 10, left panels).

Effects of 4338 on NM-induced skin damage and inflammation

Treatment of mice with 4338 beginning one hour after NM was found to mitigate tissue damage; thus, 1–3 days post NM, the size and magnitude of wound was reduced, along with inflammation (Fig. 2, Fig. 3, and Fig. 4). 4338 also prevented the formation of an eschar, and decreased overall wound thickness and epidermal hyperplasia (Fig. 3, Fig. 4, and Fig. 5). Additionally, 4338 prevented the loss of sebaceous glands, as well as collagen deposition within both the reticular and papillary dermis, and hyperkeratosis and hemorrhage within the dermis (Fig. 3, Fig. 4, and Fig. 5, right panels). This was associated with a marked reduction in iNOS and COX-2 expression as well as mast cell degranulation (Fig. 7 and Fig. 8, right panels and Fig. 9). In contrast, 4338 had no effect on PCNA expression in basal keratinocytes (Fig. 10, right panels), or on NM-induced expression of phospho-H2A.X (Fig. 6, right panels).

Discussion

Using a newly developed modified cutaneous patch model, we characterized the progression of injury and wound healing on the dorsal skin of mice following NM exposure. Initially, an inflammatory response was evident which included edema and leukocyte infiltration. This was associated with alterations in skin structure including degradation of the stratum corneum, hyperkeratosis and acanthosis, along with increased collagen deposition and hemorrhage within the dermis followed by the formation of an eschar. Subsequently, increased proliferation of keratinocytes was observed at the wound margins, which extended under the eschar initiating the formation of a neoepidermis. This generated a hyperplastic epidermis which replaced the eschar during the wound healing process. These data are consistent with earlier findings on the dermal responses of mice to sulfur mustard, as well as NM (Au et al., 2015; Casillas et al.; Jain et al., 2014; Joseph et al., 2011; Smith et al., 1997; Wormser et al.). However, in earlier studies NM was applied to the dorsal skin in large volumes of either acetone or PBS over wide areas which limited the ability to evaluate candidate therapeutics. Our studies showing that NM-induced skin injury can be localized is important, not only for characterizing the wound response, but also for quantifying the efficacy of potential mustard countermeasures.

NM is known to damage DNA causing both single and double stranded breaks (Clingen et al., 2007). Excessive DNA damage can suppress keratinocyte proliferation resulting in persistent tissue injury (Barnes et al., 2010; Inturi et al., 2014; Shahin et al., 2001). Phosphorylation of the histone H2A variant, H2A.X, which recruits DNA damage response proteins, is critical for the repair of DNA breaks (Mah et al., 2010; Scully and Xie, 2013).

Consistent with previous findings (Inturi et al., 2014; Jain et al., 2015; Joseph et al., 2011), we found that NM caused a rapid increase in phospho H2A.X in the nuclei of basal and suprabasal cells of the interfollicular epidermis and the outer root sheath of hair follicles, presumably a response to DNA damage. Two-three days post-NM, phospho-H2A.X was also evident in infiltrating neutrophils and macrophages, which are known to undergo apoptosis. High molecular weight DNA fragmentation occurs during apoptosis and this is associated with phosphorylation of H2A.X (Rogakou et al., 2000). Of interest were our findings that phospho-H2A.X persisted in basal cells of the neoepidermis for at least 5 days post NM. This suggests that despite extensive keratinocyte proliferation, DNA damage persists, which may contribute to aberrant or delayed wound repair. In this regard, sulfur mustard has been shown to prolong wound healing in human skin (Ghabili et al., 2011; Rice, 2003). It is also possible that phosphorylated H2A.X is generated during DNA replication, and it may be that rapidly dividing/differentiating keratinocytes express this modified histone during the wound healing process (Mejia-Ramirez et al., 2015; Sharma et al., 2012; Williams et al., 2010).

iNOS and COX-2, are important in generating cytotoxic pro-inflammatory mediators in the skin (Lee et al., 2003; Moncada, 1999). Constitutive expression of both enzymes was noted in sebocytes of control skin, which is consistent with a role of reactive nitrogen species and eicosanoids generated from iNOS and COX-2, respectively, in regulating sebaceous gland functioning including lipid biosynthesis (Alestas et al., 2006). Low constitutive levels of COX-2 were also noted in basal cells of the epidermis and outer root sheath cells in hair follicles in control skin where it also likely functions in epidermal homeostasis (Lee et al., 2003; Mitchell et al., 1995; Williams et al., 1999). NM exposure resulted in upregulation of iNOS and COX-2 in basal and superbasal cells after 1–3 days. Increases in COX-2 expression are consistent with previous findings that sulfur mustard, and the related half mustard, 2-chloroethyl ethyl sulfide, stimulate the release of prostaglandins from human and mouse keratinocytes, and that in mouse skin, sulfur mustard-induced injury is associated with increased COX-2 (Black et al., 2010; Joseph et al., 2011; Lefkowitz and Smith, 2002). While sebocytes continued to express iNOS and COX-2 for 1 day post NM, subsequently they degenerated. The contribution of iNOS- and COX-2-derived mediators to sebaceous gland degeneration following mustard exposure remains to be determined. Four-five days post NM, iNOS and COX-2 were localized throughout the hyperplastic neoepidermis. These data are consistent with earlier findings that iNOS is upregulated in mouse skin after exposure to the half-mustard, 2-chloroethyl ethyl sulfide (Jain et al., 2011). Early increases in COX-2 and the generation of eicosanoids in the skin are thought to be important in initiating inflammation (Lefkowitz and Smith, 2002; Vane et al., 1994). This is supported by findings that COX-2 inhibitors reduce sulfur mustard induced inflammation in a mouse ear vesicant model, and that sulfur mustard-induced inflammation is reduced in COX-2 deficient mice (Casillas et al., 2000; Wormser et al., 2004). Eicosanoids have been reported to stimulate keratinocyte growth, and it may be that elevated COX-2 in hyperplastic neoepidermis is important in wound repair (Lee et al., 2003; Nyska et al., 2001; Pentland and Needleman, 1986). This is supported by findings that the initial stages of acute inflammation in a full thickness incisional model of wound healing in mice are associated with the generation of proinflammatory prostaglandin PGE2, while wound repair is associated with production of anti-inflammatory PGD2 and its metabolites (Kapoor et al.,

2007). Our observation that iNOS is increased during wound healing are consistent with earlier studies showing that proliferating keratinocytes strongly express iNOS (Frank et al., 2002; Jain et al., 2011). Findings that wound healing is also reduced in mice treated with iNOS inhibitors and in iNOS-deficient mice are in accord with the notion that nitric oxide contributes to the regulation of wound healing (Au et al., 2015; Frank et al., 1998; Heck et al., 1992). This may be due to nitric oxide-induced stimulation of growth factor and cytokine release by keratinocytes (Frank et al., 1998).

Degranulation of mast cells is associated with the release of mediators important in inflammation and wound repair including histamine, cytokines, growth factors, chemokines and bioactive lipids (Rao and Brown, 2008; Shiota et al., 2010; Weller et al., 2006). Mast cells have been identified in the dermis, particularly in areas surrounding dermal appendages and at the basement membrane (Joseph et al., 2011; Weller et al., 2006). We found that NM-induced injury in mouse skin is associated with significant and persistent mast cell degranulation without increases in the number of mast cells in the tissue. Thus, whereas in control mouse skin only 23–36% of mast cells were degranulated, 50–85% were degranulated after NM treatment for at least 5 days. This may contribute to propagating the inflammatory response to NM-induced injury. The fact that degranulated mast cells persist at the wound site is consistent with the idea that they also contribute to the resolution of inflammation and the wound healing process (Ng, 2010; Noli and Miolo, 2001; Oehmichen et al., 2009). Our data are in accord with earlier studies showing both increases in numbers of mast cells and mast cell activation in mouse skin following sulfur mustard and half-mustard induced skin injury in hairless mice (Joseph et al., 2011; Tewari-Singh et al., 2009).

PCNA is a nuclear protein and DNA polymerase cofactor important in controlling DNA replication and repair (Moldovan et al., 2007; Park et al., 2015). PCNA was constitutively expressed in basal cells in the interfollicular epidermis and in hair follicles, consistent with the fact that proliferation of these cells is required to replace cells lost during the epidermal differentiation process. Increases in the number of cells expressing PCNA in the epidermis was evident within 1–2 days after NM exposure, during the formation of an eschar, and in the neoepidermis and hyperplastic epidermis during wound healing. These data are reflective of keratinocyte proliferation during wound repair (Laplante et al., 2001; Patel et al., 2006). Similar increases in PCNA expression during epidermal wound repair have been described in mouse skin following exposure to sulfur mustard (Joseph et al., 2011; Joseph et al., 2014).

Recent studies from our laboratory have demonstrated that a prodrug consisting of indomethacin, which targets cyclooxygenases, and an acetylcholinesterase inhibitor, which targets non-neuronal cholinergic anti-inflammatory signaling is effective in reducing sulfur mustard-induced mouse skin inflammation and injury (Chang et al., 2014; Young et al., 2010; Young et al., 2012). It is well known that the neurotransmitter, acetylcholine is produced by epithelial cells and immune cells. In the skin, acetylcholine participates in inflammation and the control of keratinocyte proliferation and differentiation (Grando et al., 1993; Schlereth et al., 2006; Wessler et al., 2015). The present studies show that our bifunctional drug (4338) is also effective in reducing NM-induced tissue injury. Thus, 4338 reduced inflammation and wounding, as indicated by the lack of eschar formation in NM-treated skin. This was associated with decreased epidermal hyperplasia and skin thickness,

number of cells expressing PCNA, and reduced numbers of degranulated mast cells and expression of iNOS and COX-2. Of interest was the fact that 4338 did not alter NM-induced DNA damage, as reflected by expression of phospho-H2A.X. NM is known to directly damage DNA; these data indicate that DNA damage is not essential for inflammation and skin injury, and that strategies designed to interfere with inflammatory signaling pathways are sufficient to mitigate, at least in part, vesicant-induced skin injury. It should be noted that the precise role of indomethacin released from 4338 in inhibiting cyclooxygenase activity in the skin is not known. Whereas COX-2 is important in regulating inflammation, COX-1 plays a role in skin homeostasis. The effects of COX-1 inhibition on wound healing in vesicant-treated skin remain to be determined.

In summary, the present studies characterize a semi-occlusive patch test model employing a glass microfiber filter delivery system to evaluate skin injury induced by vesicants. This highly reproducible model allowed us to evaluate the progression of NM-induced inflammation, expression of inflammatory proteins, tissue damage, the formation of an eschar, and wound healing. Moreover, using this model, a novel bifunctional agent (4338) was shown to be effective in reducing skin inflammation and injury. These data have potential clinical relevance as this prodrug may be further developed into an effective NM and sulfur mustard countermeasure (Shakarjian et al., 2010). The structural changes in the skin induced by NM in our patch model are consistent with the pathophysiology of sulfur mustard-induced skin injury in humans. These data indicate that our patch model can be used to investigate mechanisms of action of vesicants, and to screen for potential candidate therapeutics that can be used to mitigate vesicant toxicity.

Acknowledgments

We thank Sally Kim for technical assistance. This work was supported NIH grants AR055073, NS079249, ES004738 and ES005022.

Abbreviations

AChE	acetylcholinesterase
COX	cyclooxygenases
D/E	dermal/epidermal
H&E	hematoxylin & eosin
NM	nitrogen mustard
PCNA	proliferating cell nuclear antigen
phospho-H2A.X	phosphorylated histone H2A.X
PGE_2	prostaglandin E2
SM	sulfur mustard

References

Alestas T, Ganceviciene R, Fimmel S, Muller-Decker K, Zouboulis CC. Enzymes involved in the biosynthesis of leukotriene B4 and prostaglandin E2 are active in sebaceous glands. J. Mol. Med. (Berl.). 2006; 84:75–87. [PubMed: 16388388]

Anderson DR, Mitcheltree LW, Brobst DE, Byers SL, Merz DF, Gold MB. A vapor exposure model for neonatal mice. Toxicol. Mech. Methods. 2002; 12:59–70. [PubMed: 20597816]

Arck P, Paus R. From the brain-skin connection: the neuroendocrine-immune misalliance of stress and itch. Neuroimmunomodulation. 2006; 13:347–356. [PubMed: 17709957]

Au L, Meisch JP, Das LM, Binko AM, Boxer RS, Wen AM, Steinmetz NF, Lu KQ. Suppression of Hyperactive Immune Responses Protects against Nitrogen Mustard Injury. J. Invest. Dermatol. 2015; 135:2971–2981. [PubMed: 26288355]

Barnes L, Dumas M, Juan M, Noblesse E, Tesniere A, Schnebert S, Guillot B, Moles JP. GammaH2AX, an accurate marker that analyzes UV genotoxic effects on human keratinocytes and on human skin. Photochem. Photobiol. 2010; 86:933–941. [PubMed: 20492564]

Black AT, Hayden PJ, Casillas RP, Heck DE, Gerecke DR, Sinko PJ, Laskin DL, Laskin JD. Expression of proliferative and inflammatory markers in a full-thickness human skin equivalent following exposure to the model sulfur mustard vesicant, 2-chloroethyl ethyl sulfide. Toxicol. Appl. Pharmacol. 2010; 249:178–187. [PubMed: 20840853]

Buehler EV. Occlusive patch method for skin sensitization in guinea pigs: the Buehler method. Food Chem. Toxicol. 1994; 32:97–101. [PubMed: 8132183]

Cals-Grierson MM, Ormerod AD. Nitric oxide function in the skin. Nitric Oxide. 2004; 10:179–193. [PubMed: 15275864]

Casillas RP, Kiser RC, Truxall JA, Singer AW, Shumaker SM, Niemuth NA, Ricketts KM, Mitcheltree LW, Castrejon LR, Blank JA. Therapeutic approaches to dermatotoxicity by sulfur mustard. I. Modulaton of sulfur mustard-induced cutaneous injury in the mouse ear vesicant model. J. Appl. Toxicol. 2000; 20(Suppl. 1):S145–S151. [PubMed: 11428628]

Chang YC, Wang JD, Hahn RA, Gordon MK, Joseph LB, Heck DE, Heindel ND, Young SC, Sinko PJ, Casillas RP, Laskin JD, Laskin DL, Gerecke DR. Therapeutic potential of a non-steroidal bifunctional anti-inflammatory and anti-cholinergic agent against skin injury induced by sulfur mustard. Toxicol. Appl. Pharmacol. 2014; 280:236–244. [PubMed: 25127551]

Chew AL, Maibach HI. Occupational issues of irritant contact dermatitis. Int. Arch. Occup. Environ. Health. 2003; 76:339–346. [PubMed: 12827369]

Clingen PH, Arlett CF, Hartley JA, Parris CN. Chemosensitivity of primary human fibroblasts with defective unhooking of DNA interstrand cross-links. Exp. Cell Res. 2007; 313:753–760. [PubMed: 17188678]

Clingen PH, Wu JY, Miller J, Mistry N, Chin F, Wynne P, Prise KM, Hartley JA. Histone H2AX phosphorylation as a molecular pharmacological marker for DNA interstrand crosslink cancer chemotherapy. Biochem. Pharmacol. 2008; 76:19–27. [PubMed: 18508035]

Farage MA, Maibach HI, Andersen KE, Lachapelle JM, Kern P, Ryan C, Ely J, Kanti A. Historical perspective on the use of visual grading scales in evaluating skin irritation and sensitization. Contact Dermatitis. 2011; 65:65–75. [PubMed: 21668861]

Fischer T, Kihlman I. Patch testing technique. J. Am. Acad. Dermatol. 1989; 21:830–832. [PubMed: 2600207]

Frank S, Kampfer H, Wetzler C, Pfeilschifter J. Nitric oxide drives skin repair: novel functions of an established mediator. Kidney Int. 2002; 61:882–888. [PubMed: 11849442]

Frank S, Madlener M, Pfeilschifter J, Werner S. Induction of inducible nitric oxide synthase and its corresponding tetrahydrobiopterin-cofactor-synthesizing enzyme GTP-cyclohydrolase I during cutaneous wound repair. J. Invest. Dermatol. 1998; 111:1058–1064. [PubMed: 9856817]

Ghabili K, Agutter PS, Ghanei M, Ansarin K, Panahi Y, Shoja MM. Sulfur mustard toxicity: history, chemistry, pharmacokinetics, and pharmacodynamics. Crit. Rev. Toxicol. 2011; 41:384–403. [PubMed: 21329486]

Ghabili K, Agutter PS, Ghanei M, Ansarin K, Shoja MM. Mustard gas toxicity: the acute and chronic pathological effects. J. Appl. Toxicol. 2010; 30:627–643. [PubMed: 20836142]

Grando SA, Kist DA, Qi M, Dahl MV. Human keratinocytes synthesize, secrete, and degrade acetylcholine. J. Invest. Dermatol. 1993; 101:32–36. [PubMed: 8331294]

Heck DE, Laskin DL, Gardner CR, Laskin JD. Epidermal growth factor suppresses nitric oxide and hydrogen peroxide production by keratinocytes. Potential role for nitric oxide in the regulation of wound healing. J. Biol. Chem. 1992; 267:21277–21280. [PubMed: 1383221]

Hojer J, Personne M, Hulten P, Ludwigs U. Topical treatments for hydrofluoric acid burns: a blind controlled experimental study. J. Toxicol. Clin. Toxicol. 2002; 40:861–866. [PubMed: 12507055]

Hulten P, Hojer J, Ludwigs U, Janson A. Hexafluorine vs. standard decontamination to reduce systemic toxicity after dermal exposure to hydrofluoric acid. J. Toxicol. Clin. Toxicol. 2004; 42:355–361. [PubMed: 15461243]

Inturi S, Tewari-Singh N, Agarwal C, White CW, Agarwal R. Activation of DNA damage repair pathways in response to nitrogen mustard-induced DNA damage and toxicity in skin keratinocytes. Mutat. Res. 2014; 763–764:53–63.

Jain AK, Tewari-Singh N, Gu M, Inturi S, White CW, Agarwal R. Sulfur mustard analog, 2-chloroethyl ethyl sulfide-induced skin injury involves DNA damage and induction of inflammatory mediators, in part via oxidative stress, in SKH-1 hairless mouse skin. Toxicol. Lett. 2011; 205:293–301. [PubMed: 21722719]

Jain AK, Tewari-Singh N, Inturi S, Kumar D, Orlicky DJ, Agarwal C, White CW, Agarwal R. Flavanone silibinin treatment attenuates nitrogen mustard-induced toxic effects in mouse skin. Toxicol. Appl. Pharmacol. 2015; 285:71–78. [PubMed: 25791923]

Jain AK, Tewari-Singh N, Inturi S, Orlicky DJ, White CW, Agarwal R. Histopathological and immunohistochemical evaluation of nitrogen mustard-induced cutaneous effects in SKH-1 hairless and C57BL/6 mice. Exp. Toxicol. Pathol. 2014; 66:129–138. [PubMed: 24373750]

Joseph LB, Gerecke DR, Heck DE, Black AT, Sinko PJ, Cervelli JA, Casillas RP, Babin MC, Laskin DL, Laskin JD. Structural changes in the skin of hairless mice following exposure to sulfur mustard correlate with inflammation and DNA damage. Exp. Mol. Pathol. 2011; 91:515–527. [PubMed: 21672537]

Joseph LB, Heck DE, Cervelli JA, Composto GM, Babin MC, Casillas RP, Sinko PJ, Gerecke DR, Laskin DL, Laskin JD. Structural changes in hair follicles and sebaceous glands of hairless mice following exposure to sulfur mustard. Exp. Mol. Pathol. 2014; 96:316–327. [PubMed: 24662110]

Jowsey PA, Williams FM, Blain PG. DNA damage, signalling and repair after exposure of cells to the sulphur mustard analogue 2-chloroethyl ethyl sulphide. Toxicology. 2009; 257:105–112. [PubMed: 19111594]

Kapoor M, Kojima F, Yang L, Crofford LJ. Sequential induction of pro- and anti-inflammatory prostaglandins and peroxisome proliferators-activated receptor-gamma during normal wound healing: a time course study. Prostaglandins Leukot. Essent. Fat. Acids. 2007; 76:103–112.

Laplante AF, Germain L, Auger FA, Moulin V. Mechanisms of wound reepithelialization: hints from a tissue-engineered reconstructed skin to long-standing questions. FASEB J. 2001; 15:2377–2389. [PubMed: 11689463]

Lee JL, Mukhtar H, Bickers DR, Kopelovich L, Athar M. Cyclooxygenases in the skin: pharmacological and toxicological implications. Toxicol. Appl. Pharmacol. 2003; 192:294–306. [PubMed: 14575647]

Lefkowitz LJ, Smith WJ. Sulfur mustard-induced arachidonic acid release is mediated by phospholipase D in human keratinocytes. Biochem. Biophys. Res. Commun. 2002; 295:1062–1067. [PubMed: 12135602]

Mah LJ, El-Osta A, Karagiannis TC. gammaH2AX: a sensitive molecular marker of DNA damage and repair. Leukemia. 2010; 24:679–686. [PubMed: 20130602]

Mejia-Ramirez E, Limbo O, Langerak P, Russell P. Critical Function of gammaH2A in S-Phase. PLoS Genet. 2015; 11:e1005517. [PubMed: 26368543]

Mershon MM, Mitcheltree LW, Petrali JP, Braue EH, Wade JV. Hairless guinea pig bioassay model for vesicant vapor exposures. Fundam. Appl. Toxicol. 1990; 15:622–630. [PubMed: 2258024]

Mitchell JA, Larkin S, Williams TJ. Cyclooxygenase-2: regulation and relevance in inflammation. Biochem. Pharmacol. 1995; 50:1535–1542. [PubMed: 7503754]

Moldovan GL, Pfander B, Jentsch S. PCNA, the maestro of the replication fork. Cell. 2007; 129:665–679. [PubMed: 17512402]

Moncada S. Nitric oxide: discovery and impact on clinical medicine. J. RSoc. Med. 1999; 92:164–169.

Ng MF. The role of mast cells in wound healing. Int. Wound J. 2010; 7:55–61. [PubMed: 20409251]

Nicholson M, Willis CM. The influence of patch test size and design on the distribution of erythema induced by sodium lauryl sulfate. Contact Dermatitis. 1999; 41:264–267. [PubMed: 10554060]

Noli C, Miolo A. The mast cell in wound healing. Vet. Dermatol. 2001; 12:303–313. [PubMed: 11844219]

Nyska A, Lomnitski L, Maronpot R, Moomaw C, Brodsky B, Sintov A, Wormser U. Effects of iodine on inducible nitric oxide synthase and cyclooxygenase-2 expression in sulfur mustard-induced skin. Arch. Toxicol. 2001; 74:768–774. [PubMed: 11305779]

Oehmichen M, Gronki T, Meissner C, Anlauf M, Schwark T. Mast cell reactivity at the margin of human skin wounds: an early cell marker of wound survival? Forensic Sci. Int. 2009; 191:1–5. [PubMed: 19560296]

Park SY, Jeong MS, Han CW, Yu HS, Jang SB. Structural and functional insight into proliferating cell nuclear antigen. J. Microbiol. Biotechnol. 2015; 26:637–642. [PubMed: 26699741]

Patel GK, Wilson CH, Harding KG, Finlay AY, Bowden PE. Numerous keratinocyte subtypes involved in wound re-epithelialization. J. Invest. Dermatol. 2006; 126:497–502. [PubMed: 16374449]

Pentland AP, Needleman P. Modulation of keratinocyte proliferation in vitro by endogenous prostaglandin synthesis. J. Clin. Invest. 1986; 77:246–251. [PubMed: 3080474]

Rao KN, Brown MA. Mast cells: multifaceted immune cells with diverse roles in health and disease. Ann. N. YAcad. Sci. 2008; 1143:83–104.

Rice P. Sulphur mustard injuries of the skin. Pathophysiology and management. Toxicol Rev. 2003; 22:111–118. [PubMed: 15071821]

Rogakou EP, Nieves-Neira W, Boon C, Pommier Y, Bonner WM. Initiation of DNA fragmentation during apoptosis induces phosphorylation of H2AX histone at serine 139. J. Biol. Chem. 2000; 275:9390–9395. [PubMed: 10734083]

Schlereth T, Birklein F, an Haack K, Schiffmann S, Kilbinger H, Kirkpatrick CJ, Wessler I. In vivo release of non-neuronal acetylcholine from the human skin as measured by dermal microdialysis: effect of botulinum toxin. Br. J. Pharmacol. 2006; 147:183–187. [PubMed: 16273117]

Scully R, Xie A. Double strand break repair functions of histone H2AX. Mutat. Res. 2013; 750:5–14. [PubMed: 23916969]

Shahin S, Cullinane C, Gray PJ. Mitochondrial and nuclear DNA damage induced by sulphur mustard in keratinocytes. Chem. Biol. Interact. 2001; 138:231–245. [PubMed: 11714481]

Shakarjian MP, Heck DE, Gray JP, Sinko PJ, Gordon MK, Casillas RP, Heindel ND, Gerecke DR, Laskin DL, Laskin JD. Mechanisms mediating the vesicant actions of sulfur mustard after cutaneous exposure. Toxicol. Sci. 2010; 114:5–19. [PubMed: 19833738]

Sharma A, Singh K, Almasan A. Histone H2AX phosphorylation: a marker for DNA damage. Methods Mol. Biol. 2012; 920:613–626. [PubMed: 22941631]

Shiota N, Nishikori Y, Kakizoe E, Shimoura K, Niibayashi T, Shimbori C, Tanaka T, Okunishi H. Pathophysiological role of skin mast cells in wound healing after scald injury: study with mast cell-deficient W/W(V) mice. Int. Arch. Allergy Immunol. 2010; 151:80–88. [PubMed: 19672099]

Simon GA, Maibach HI. Relevance of hairless mouse as an experimental model of percutaneous penetration in man. Skin Pharmacol. Appl. Ski. Physiol. 1998; 11:80–86.

Smith KJ, Casillas R, Graham J, Skelton HG, Stemler F, Hackley BE Jr. Histopathologic features seen with different animal models following cutaneous sulfur mustard exposure. J. Dermatol. Sci. 1997; 14:126–135. [PubMed: 9039976]

Tewari-Singh N, Jain AK, Inturi S, White CW, Agarwal R. Clinically-relevant cutaneous lesions by nitrogen mustard: useful biomarkers of vesicants skin injury in SKH-1 hairless and C57BL/6 mice. PLoS One. 2013; 8:e67557. [PubMed: 23826320]

Tewari-Singh N, Jain AK, Orlicky DJ, White CW, Agarwal R. Cutaneous injury-related structural changes and their progression following topical nitrogen mustard exposure in hairless and haired mice. PLoS One. 2014; 9:e85402. [PubMed: 24416404]

Tewari-Singh N, Rana S, Gu M, Pal A, Orlicky DJ, White CW, Agarwal R. Inflammatory biomarkers of sulfur mustard analog 2-chloroethyl ethyl sulfide-induced skin injury in SKH-1 hairless mice. Toxicol. Sci. 2009; 108:194–206. [PubMed: 19075041]

Vane JR, Mitchell JA, Appleton I, Tomlinson A, Bishop-Bailey D, Croxtall J, Willoughby DA. Inducible isoforms of cyclooxygenase and nitric-oxide synthase in inflammation. Proc. Natl. Acad. Sci. U. S. A. 1994; 91:2046–2050. [PubMed: 7510883]

Vieille-Petit A, Blickenstaff N, Coman G, Maibach H. Metrics and clinical relevance of percutaneous penetration and lateral spreading. Skin Pharmacol. Physiol. 2015; 28:57–64. [PubMed: 25227720]

Vogt RF Jr, Dannenberg AM Jr, Schofield BH, Hynes NA, Papirmeister B. Pathogenesis of skin lesions caused by sulfur mustard. Fundam. Appl. Toxicol. 1984; 4:S71–S83. [PubMed: 6233199]

Weller K, Foitzik K, Paus R, Syska W, Maurer M. Mast cells are required for normal healing of skin wounds in mice. FASEB J. 2006; 20:2366–2368. [PubMed: 16966487]

Wessler I, Michel-Schmidt R, Kirkpatrick CJ. pH-dependent hydrolysis of acetylcholine: Consequences for non-neuronal acetylcholine. Int. Immunopharmacol. 2015; 29:27–30. [PubMed: 25929445]

Williams CS, Mann M, DuBois RN. The role of cyclooxygenases in inflammation, cancer, and development. Oncogene. 1999; 18:7908–7916. [PubMed: 10630643]

Williams JS, Williams RS, Dovey CL, Guenther G, Tainer JA, Russell P. gammaH2A binds Brc1 to maintain genome integrity during S-phase. EMBO J. 2010; 29:1136–1148. [PubMed: 20094029]

Wormser U, Langenbach R, Peddada S, Sintov A, Brodsky B, Nyska A. Reduced sulfur mustard-induced skin toxicity in cyclooxygenase-2 knockout and celecoxib-treated mice. Toxicol. Appl. Pharmacol. 2004; 200:40–47. [PubMed: 15451306]

Young S, Fabio K, Guillon C, Mohanta P, Halton TA, Heck DE, Flowers RA 2nd, Laskin JD, Heindel ND. Peripheral site acetylcholinesterase inhibitors targeting both inflammation and cholinergic dysfunction. Bioorg. Med. Chem. Lett. 2010; 20:2987–2990. [PubMed: 20347302]

Young SC, Fabio KM, Huang MT, Saxena J, Harman MP, Guillon CD, Vetrano AM, Heck DE, Flowers RA 2nd, Heindel ND, Laskin JD. Investigation of anticholinergic and non-steroidal anti-inflammatory prodrugs which reduce chemically induced skin inflammation. J. Appl. Toxicol. 2012; 32:135–141. [PubMed: 21319177]

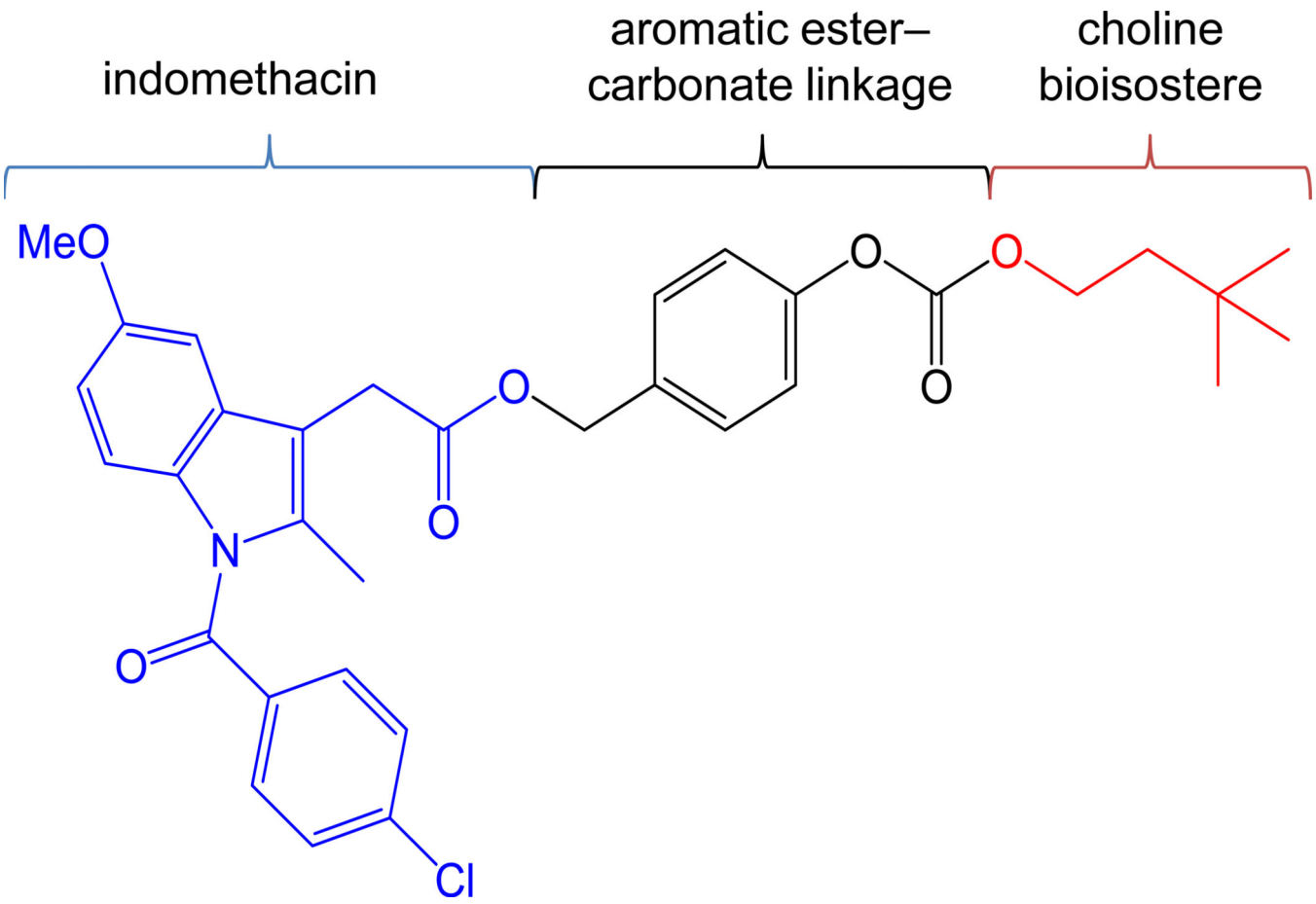

Fig. 1. Chemical structure of 4338

4338 consists of an anti-inflammatory moiety, indomethacin, and a choline bioisostere 3,3-dimethyl-1-butanol, linked via an aromatic ester–carbonate.

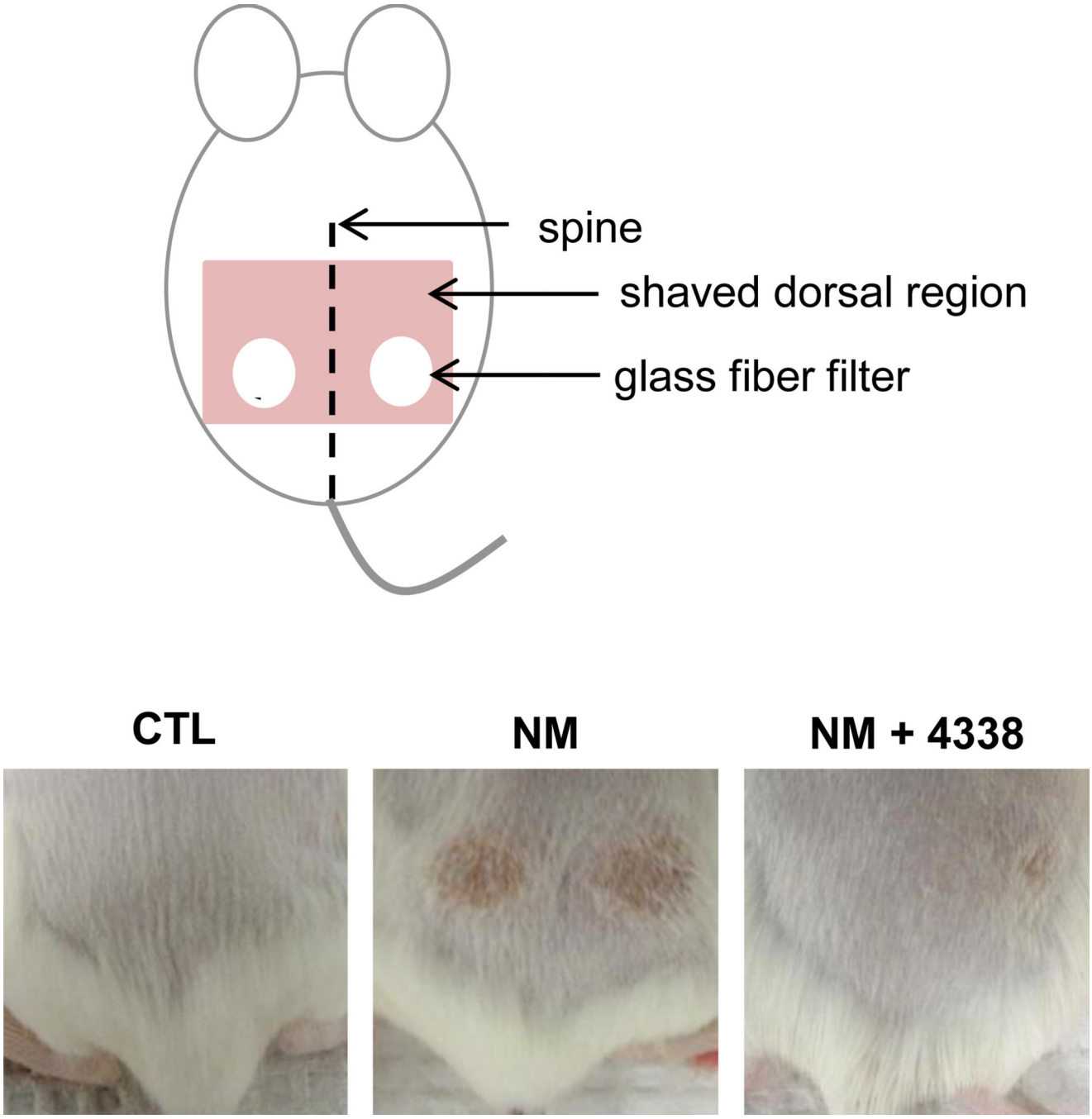

Fig. 2. Modified dorsal skin patch model

The dorsal skin of CD-1 mice was shaved and 6 mm glass fiber filter discs placed on the lumbar region of the skin equal distant from the spine (upper panel). Twenty microliters of a 1 M solution of NM in 20% deionized water/80% acetone (v/v) or vehicle control was applied to the filters which were then covered with PARAFILM®. After 6 min, the filter discs were removed and the skin analyzed for tissue damage 1–5 days post exposure. Mice were treated with 4338 four times per day beginning 1 h post NM exposure. The lower panel shows the skin from control (CTL), NM and NM + 4338 treated skin 3 days post NM.

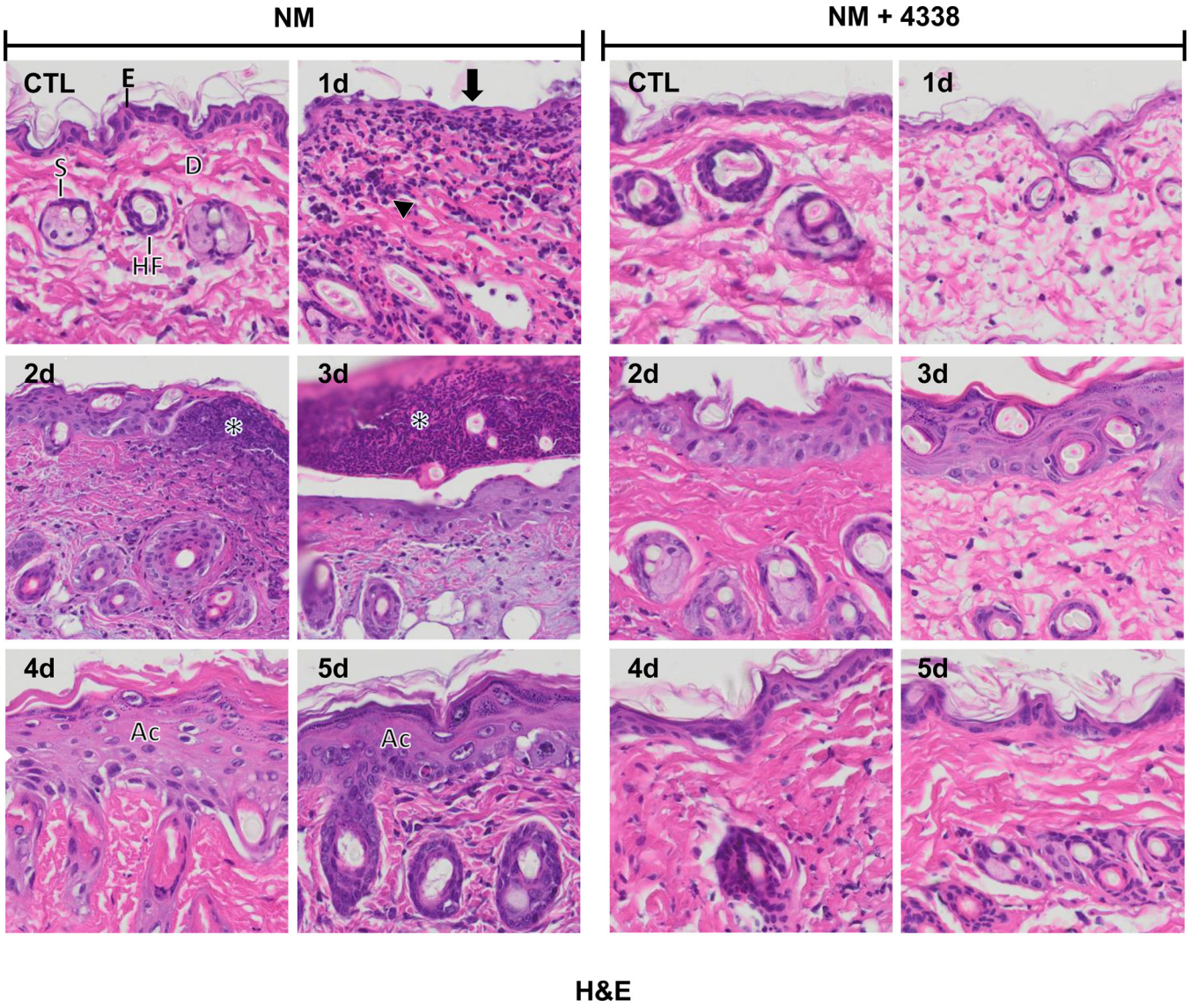

Fig. 3. Hematoxylin and eosin staining of mouse skin following NM exposure

Histological sections, prepared from control (CTL) mouse skin and mouse skin 1–5 days post NM exposure, were stained with hematoxylin and eosin, which stains nuclei blue/black, and keratin and cytoplasm red. One representative section from 3 mice/treatment group is shown (original magnification, × 400). E, epidermis; D, dermis; S, sebaceous gland; HF, hair follicle; asterisk, eschar, Ac, acanthosis. Black arrow, loss of stratum corneum; black arrowhead, inflammatory cell infiltrate. Left panels, mouse skin treated with NM; right panels, mouse skin treated with NM and 4338.

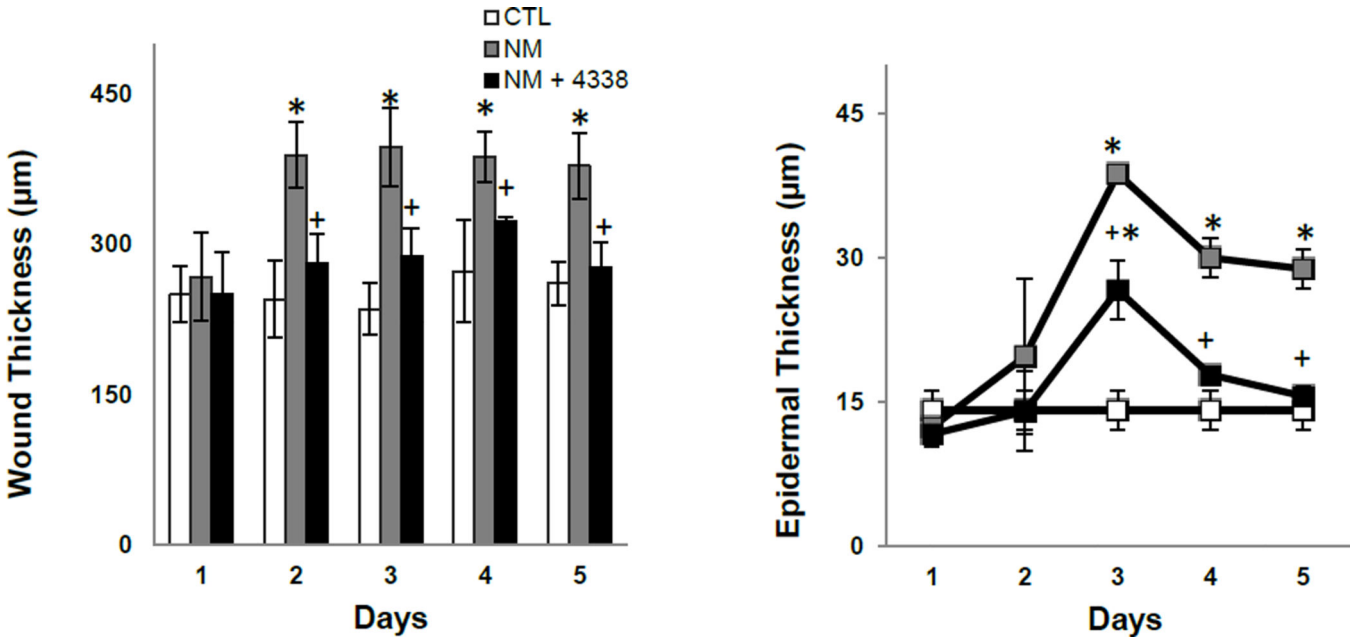

Fig. 4. Effects of NM on mouse skin wound and epidermal thickness

Histological sections, prepared from control (CTL) mouse skin and mouse skin collected 1–5 days post NM, were stained with hematoxylin and eosin and wound (left panel) and epidermal (right panel) thickness assessed as described in the Materials and Methods Section. Each point represents the mean ± SE ($n = 6$). *Significantly different from control mouse skin ($p \leq 0.05$); $^{+}$Significantly different from NM treated mouse skin.

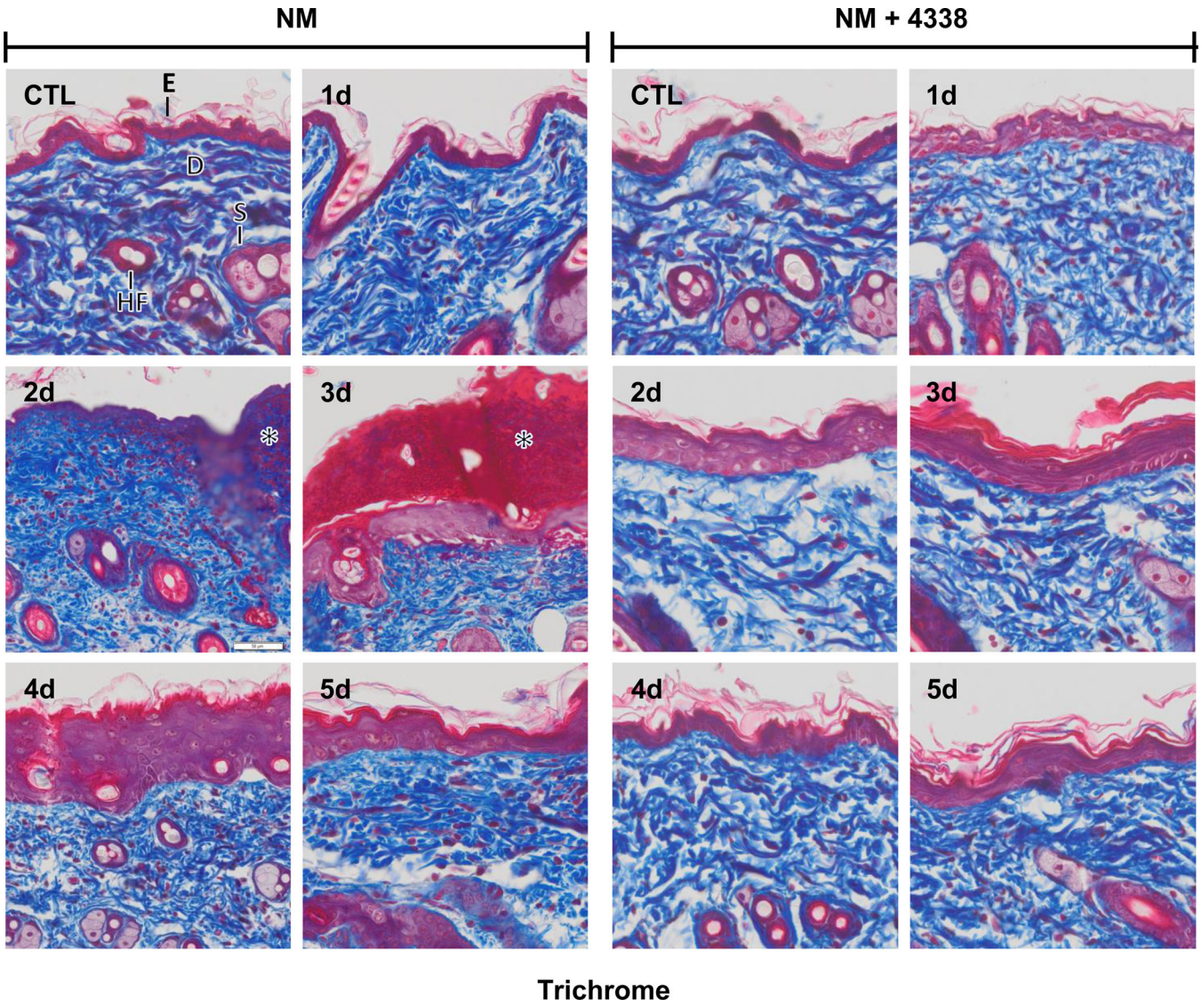

Fig. 5. Trichrome staining of mouse skin following exposure to NM

Histological sections, prepared from control (CTL) mouse skin and mouse skin 1–5 days post NM exposure, were stained with Gomori's trichrome containing hematoxylin, which stains nuclei blue/black, eosin which stains keratin and cytoplasm red, and aniline blue which stains collagen I/III royal blue. One representative section from 3 mice/treatment group is shown (original magnification, × 400). E, epidermis; D, dermis; S, sebaceous gland; HF, hair follicle; asterisk, eschar; star, collagen deposition. Left panels, mouse skin treated with NM; right panels, mouse skin treated with NM and 4338.

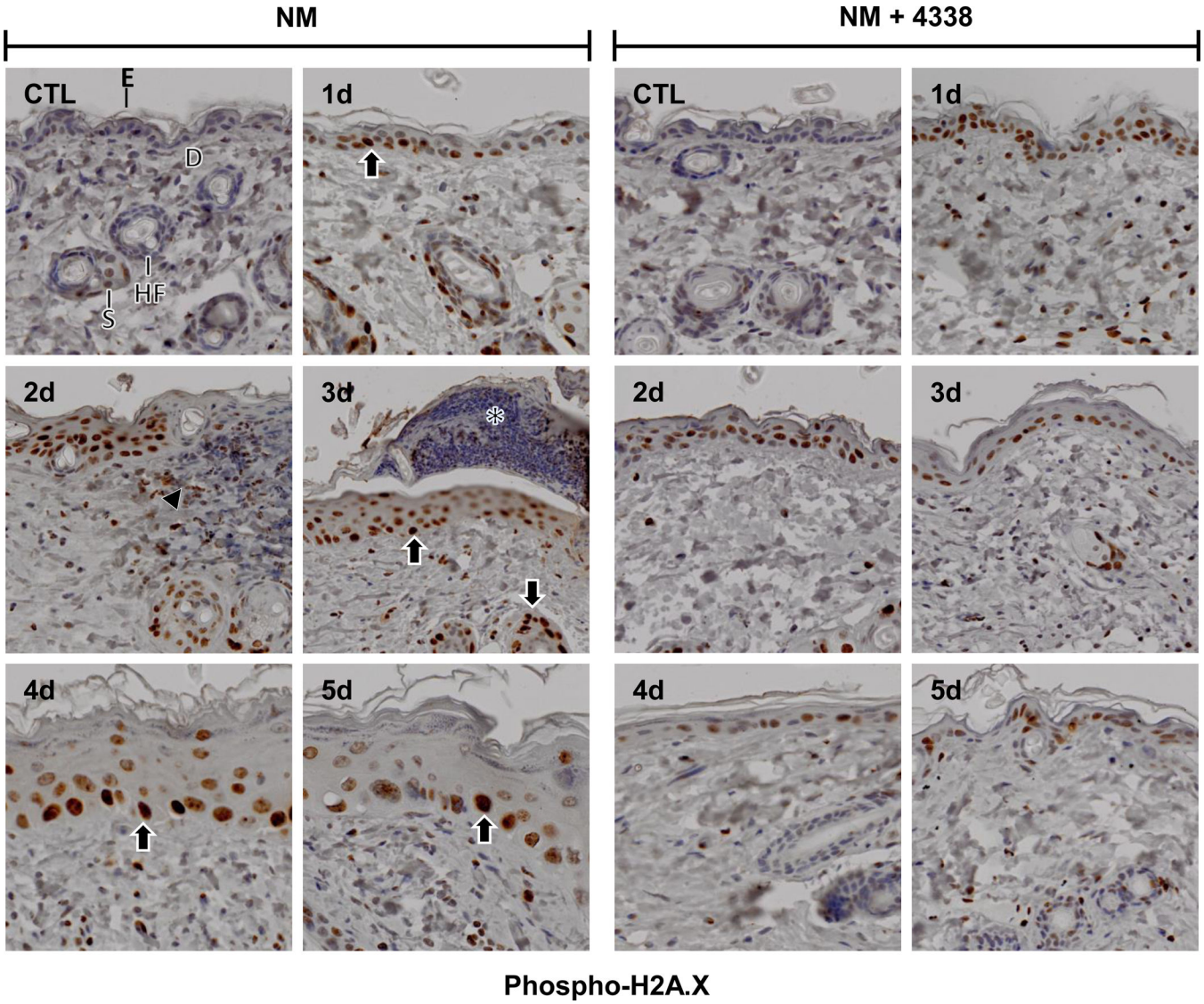

Fig. 6. Effects of NM on phospho-H2A.X expression in mouse skin

Histological sections, prepared from control (CTL) mouse skin and mouse skin 1–5 days post NM, were stained with an antibody to phospho-H2A.X. Antibody binding was visualized using a Vectastain Elite ABC kit. One representative section from 3 mice/treatment group is shown (original magnification,× 400). E, epidermis; D, dermis; S, sebaceous gland; HF, hair follicle; asterisk, eschar. Black arrow, keratinocytes expressing phospho-H2A.X. Black arrowhead, inflammatory cell infiltrate. Left panels, mouse skin treated with NM; right panels, mouse skin treated with NM and 4338.

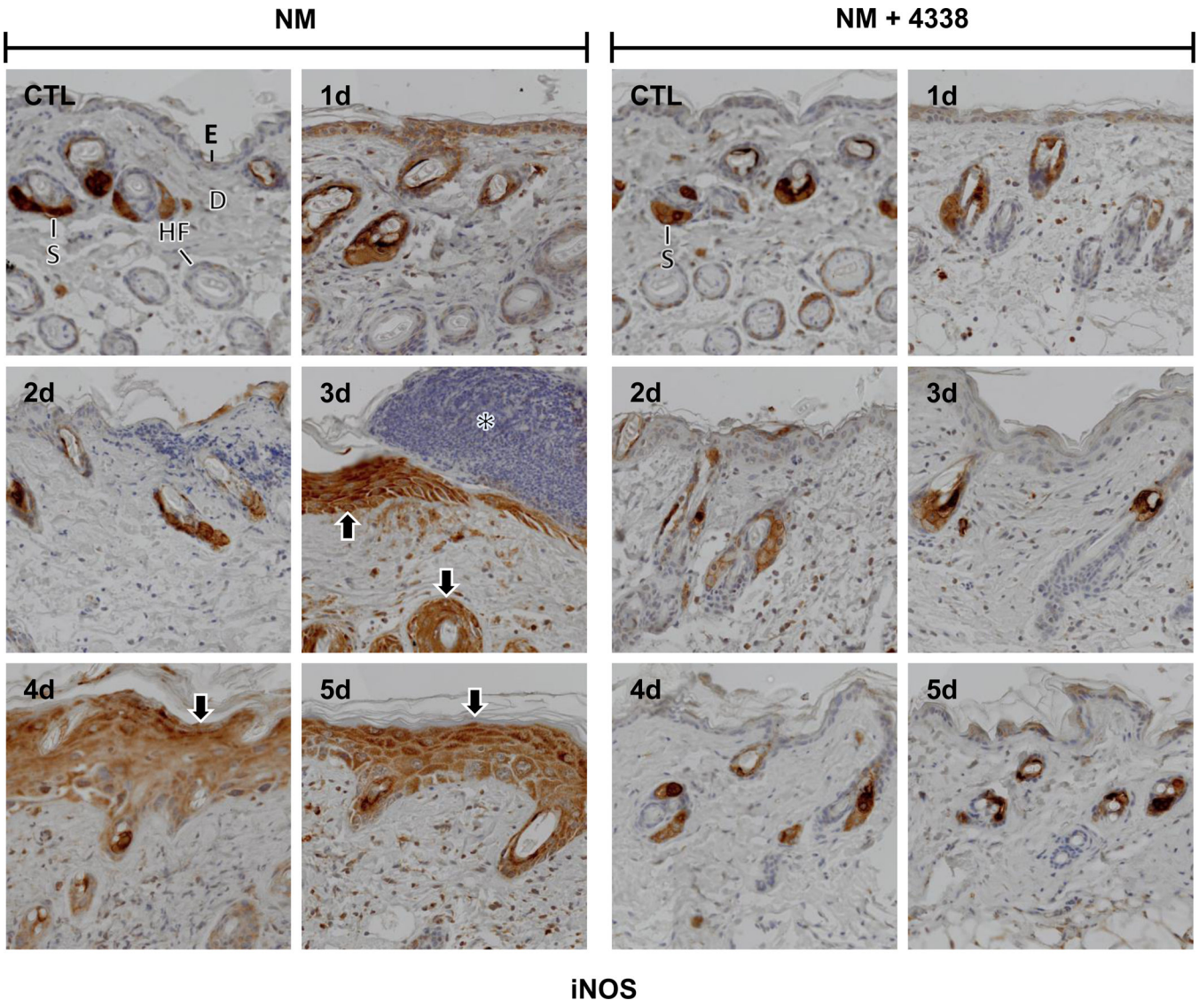

Fig. 7. Effects of NM on iNOS expression in mouse skin

Histological sections, prepared from control (CTL) mouse skin and mouse skin 1–5 days post NM, were stained with an antibody to iNOS. Antibody binding was visualized using a Vectastain Elite ABC kit. One representative section from 3 mice/treatment group is shown (original magnification, × 400). E, epidermis; D, dermis; S, sebaceous gland; HF, hair follicle; asterisk, eschar. Black arrows, keratinocyte expression of iNOS. Left panels, mouse skin treated with NM; right panels, mouse skin treated with NM and 4338.

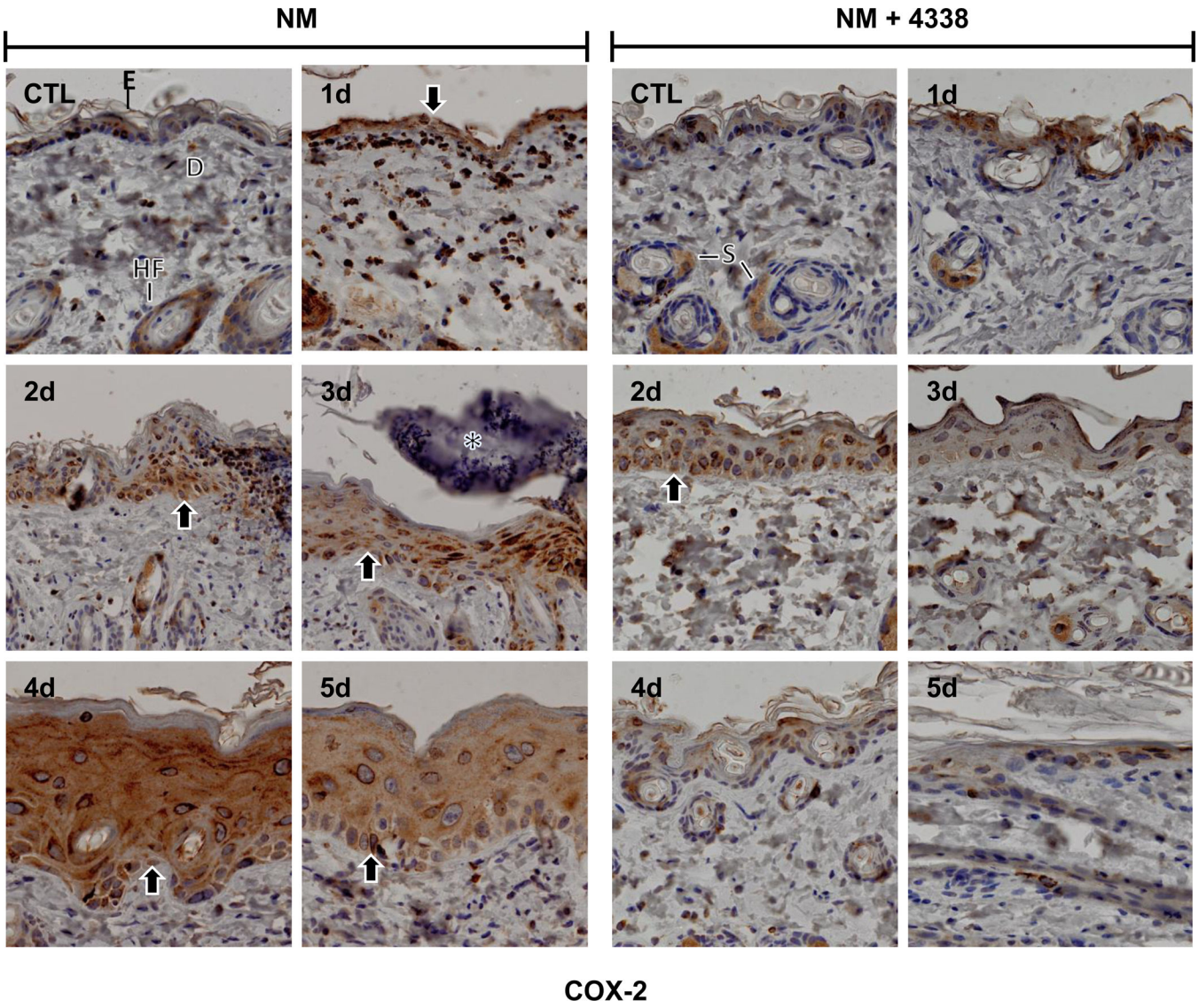

Fig. 8. Effects of NM on COX-2 expression in mouse skin

Histological sections, prepared from control (CTL) mouse skin and mouse skin 1–5 days post NM, were stained with an antibody to COX-2. Antibody binding was visualized using a Vectastain Elite ABC kit. One representative section from 3 mice/treatment group is shown (original magnification, × 400).). E, epidermis; D, dermis; S, sebaceous gland; HF, hair follicle; asterisk, eschar. Black arrows, keratinocyte expression of COX-2. Left panels, mouse skin treated with NM; right panels, mouse skin treated with NM and 4338.

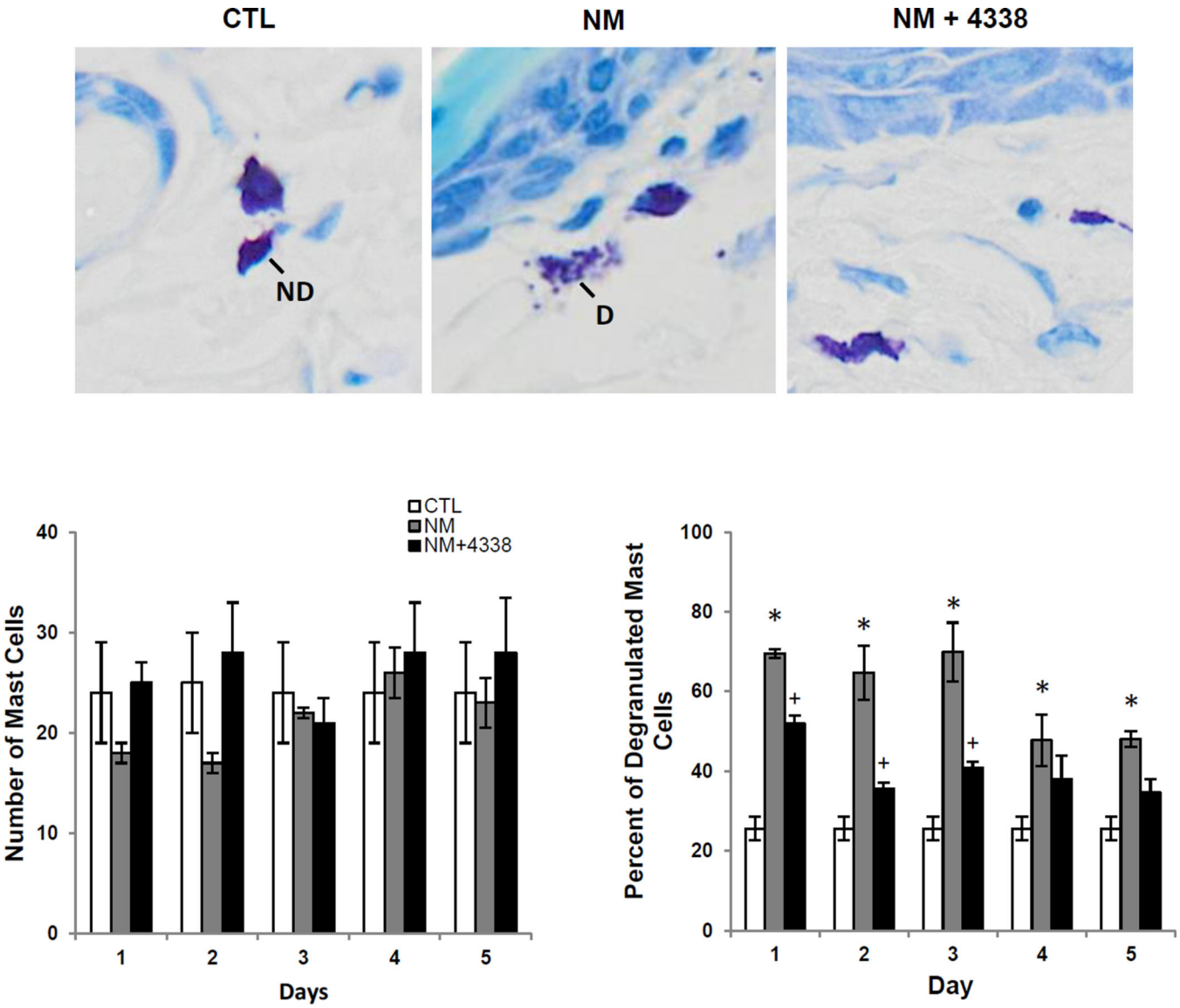

Fig. 9. Effects of NM on mast cell degranulation

Histologic sections prepared from control (CTL) mouse skin and mouse skin 3 days post NM or NM + 4338 were stained for mast cells using toluidine blue (upper panels, original magnification, × 400). Insets show intact and degranulated mast cells in control skin and NM treated skin, ND, no degranulation; D, degranulation. Lower panel shows the number of mast cells at the dermal/epidermal (D/E) junction in control, NM and NM + 4338 treated skin (lower left panel) and the percentage of mast cells that were degranulated (lower right panel). Each bar is the mean ± S.E. ($n = 3$). of 10 fields at 40× mag. *Significantly different from control ($p \leq 0.05$); $^{+}$Significantly different from NM treatment.

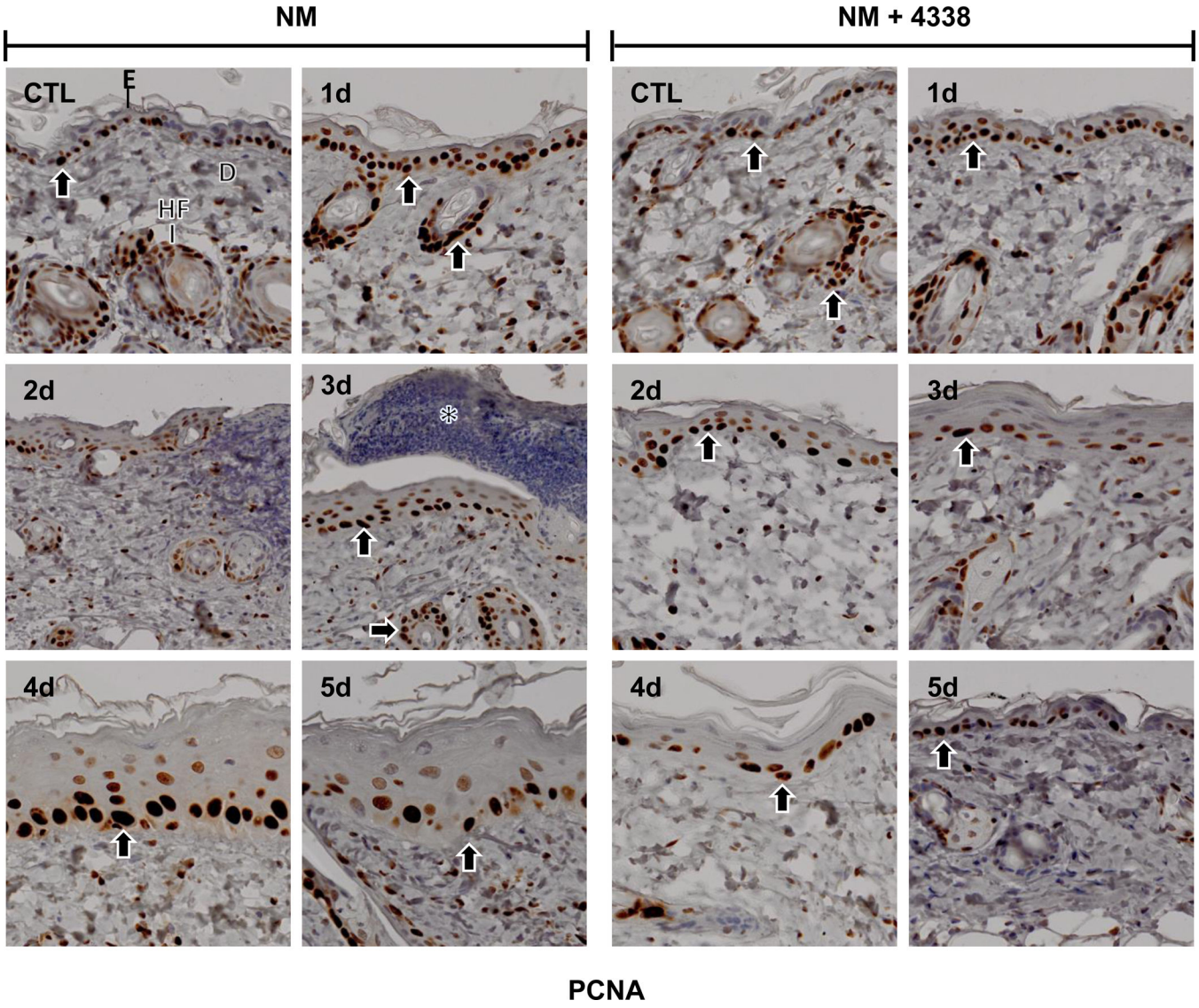

Fig. 10. Effects of NM on PCNA expression in mouse skin

Histological sections, prepared from control (CTL) skin and skin 1–5 days post NM, were stained with an antibody to PCNA. Antibody binding was visualized using a Vectastain Elite ABC kit (original magnification, × 400). One representative section from 3 mice/treatment group is shown. E, epidermis; D, dermis; HF, hair follicle; asterisk, eschar. Black arrows, keratinocyte expression of PCNA. Left panels, mouse skin treated with NM; right panels, mouse skin treated with NM and 4338.